Magnetic Behavior of Twin Roller Melt Spun $Cu_{90}Co_{10}$ Alloys

Henry Núñez Coavas[1], Gabriela Pozo López[1,2], Luis M. Fabietti[1,2], Adriana M. Condó[3], and Silvia E. Urreta[1]

[1]Facultad de Matemática, Astronomía y Física, Universidad Nacional de Córdoba, Córdoba 5000, Argentina
[2]Instituto de Física Enrique Gaviola, CONICET, Argentina
[3]Centro Atómico Bariloche, Comisión Nacional de Energía Atómica—Instituto Balseiro, Universidad Nacional de Cuyo, CONICET, Bariloche, Argentina

Magnetoresistive $Cu_{90}Co_{10}$ alloys have been produced by twin roller melt spinning at tangential wheel speeds between 10 m/s and 30 m/s to obtain different solute and Co-rich precipitate distributions. X-ray diffraction indicates that the ribbons are polycrystalline with a fcc Cu(Co) (200) textured matrix; no evidence of a spinodal-like composition modulation could be detected with this technique. Transmission electron microscopy observations performed in samples quenched at 10 m/s indicate the existence of small, coherent, Co-rich precipitates of mean size of about 11 nm and bigger ($\sim$40 nm) Co-oxide particles. The small coherent precipitates form colonies inside the grains, mediated by precipitate free zones. Samples quenched at 30 m/s are single magnetic phase (superparamagnetic), but the hysteresis loops of the other as cast ribbons are well fitted by a superparamagnetic contribution and a ferromagnetic one, the latter arising from the Co-rich precipitates. Room temperature coercivities, of about 30–50 mT, are lower than those predicted for a mechanism of coherent rotation in the ensemble of non-interacting, Co-rich precipitates.

***Index Terms*—Magnetic properties, melt spinning, precipitation, spinodal decomposition.**

I. Introduction

DIFFERENT ultra rapid solidification techniques have been successfully applied to obtain $Cu_{90}Co_{10}$ alloys exhibiting giant magnetoresistance (GMR) [1]. The process generally involves two stages: the alloy is first fast cooled from the melt and then further annealed to achieve the optimal microstructure leading to GMR [1]–[6]. Recently, relatively large GMR values [7] and a low temperature Kondo-like effect [8] have been observed in as cast samples, processed by twin roller melt spinning. The GMR and the Kondo-like effects are both attributed to spin-dependent scattering mechanisms involving small magnetic Co clusters/precipitates finely dispersed in the Cu-rich matrix. Then, there is a clear key role of precipitates in determining important properties in this alloy.

The twin roller processing technique imposes symmetric heat extraction conditions during solidification, allowing one to obtain quite uniform microstructures quenched at relatively low rates (samples slowly cooled in a conventional melt spinning process exhibit a quite heterogeneous structure). In the present work, we explore the microstructure and the resulting magnetic properties of a $Cu_{90}Co_{10}$ alloy processed by twin roller melt spinning at different substrate speeds, keeping the wheels in contact by a known force of 24 N. We focus our investigation on the precipitation microstructure in the as cast state and on the magnetic behavior of these microstructures.

II. Experimental Procedure

A master alloy of nominal composition $Cu_{90}Co_{10}$ was prepared by arc melting; the small ingots so obtained were further remelted four times to improve homogenization. All these procedures were conducted under a Zr gettered Ar atmosphere. The alloy was further processed in a twin roller melt spinning device at three different tangential wheel speeds: 10, 20, and 30 m/s to obtain samples V10, V20, and V30, respectively. The resulting ribbons were characterized by X-ray diffraction (XRD) and transmission electron microscopy (TEM). XRD profiles were recorded in a Philips PW 1710/01 diffractometer in the 2θ range from 20° to 100°, in Bragg-Brentano configuration, using Cu Kα radiation ($\lambda = 1.5418$ Å). TEM thin foils were prepared by twin-jet electropolishing with an electrolyte containing 500 ml distilled water, 250 ml ethanol, 250 ml orthophosphoric acid, 50 ml propilic alcohol and 5 g urea. TEM observations and selected area diffraction patterns were performed in a Philips CM 200 UT microscope, operating at 200 kV and equipped with energy-dispersive X-ray spectroscopy (EDS) facility. Magnetic measurements were performed in 6 mm long as-cast ribbons with the applied field parallel to the sample length. The demagnetizing factors N, resulted about 0.017 ± 0.004, leading to internal fields quite similar to the applied field. Room temperature magnetic hysteresis loops were measured in a vibrating sample magnetometer (VSM) Lakeshore 7300, with a maximum field up to 1.5 T. The magnetic polarization as a function temperature was measured in a Quantum Design SQUID magnetometer, under an applied field of 10 mT (100 Oe) in the temperature range of 5 K–300 K.

III. Results and Discussion

X-ray diffractograms corresponding to samples quenched at different rates are shown in Fig. 1. As previously reported [7], [8], the main phase is a fcc Cu(Co) alloy while a minor fcc Co-rich phase (P) is also detected; in addition, quite small peaks of fcc CoO (antiferromagnetic, Neel temperature 290 K) are observed together with an unindexed phase/s indicated with a "?" on the plot. The lattice parameters of the matrix and the minor phase were calculated by fitting to the structural reflections 111, 200, 220, 311 and 222 a Pearson VII profile after correcting the zero shift effect. No evidence of a spinodal decomposition could be detected with this technique. Approximate values for

Manuscript received February 16, 2013; revised March 27, 2013; accepted April 16, 2013. Date of current version July 23, 2013. Corresponding author: S. E. Urreta (e-mail: urreta@famaf.unc.edu.ar).

Color versions of one or more of the figures in this paper are available online at http://ieeexplore.ieee.org.

Digital Object Identifier 10.1109/TMAG.2013.2259618

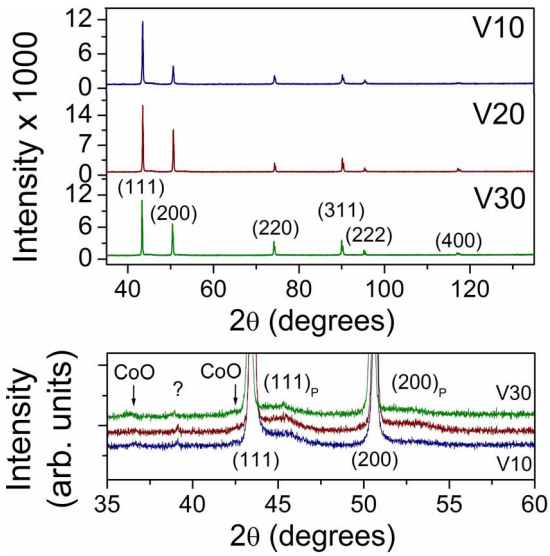

Fig. 1. XRD patterns corresponding to the alloy quenched at different substrate speeds. Major phase is fcc Cu(Co) solid solution. Minor Co or Co-rich phase is detected (coherent precipitates, P) together with an oxide phase, CoO (indicated by arrows); unknown phase/s are indicated by a "?".

TABLE I
PARAMETERS ESTIMATED FROM XRD DATA

Sample	a_{0m} [Å]	a_{0P} [Å]	e_m [10^{-4}]	e_P [10^{-3}]
V10	3.6107(5)	3.50(1)	15(2)	40(8)
V20	3.6128(5)	3.50(2)	5(1)	36(5)
V30	3.6113(5)	3.49(2)	5(2)	34(3)

Lattice constant and the mean internal strain of the matrix phase, a_{0m} and e_m, and of the minor phase a_{0P} and e_P. Numbers between brackets are errors in the last significant digit.

the mean lattice strain e were determined using the Stokes and Wilson relation: $e = \beta/(4\tan\theta)$, from measurements of the integral breath β of the diffraction lines after correcting for instrumental broadening; the values corresponding to the phases investigated are indicated in Table I. XRD line analysis was not used to estimate the crystallite size of the different phases; for the minor phase, the Scherrer formula led to values smaller than 5 nm in all the samples, with a huge error associated. Moreover, the grain size of the major phase was well above 100 nm, a range where this formulae is not applicable.

The alloys obtained by this new procedure were further investigated with TEM and the microstructure details of sample V10 are illustrated in Fig. 2. It is a bright field image under two-beam condition with $\mathbf{g} = 002$ (in the diffraction pattern only the transmitted spot and the 002 diffraction spot have appreciable intensity); in this condition, coherent precipitates show typical butterfly diffraction contrast due to lattice mismatch with the matrix (Ashby-Brown contrast: lattice-strain effects around spherical precipitates appear as lobes of low intensity with a line of no contrast perpendicular to $\mathbf{g}$).

Cu(Co) precipitates are not uniformly distributed in the matrix grains but form colonies, mediated by precipitate-free zones. This microstructure feature has not been previously

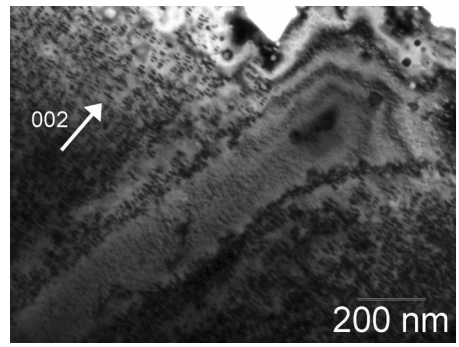

Fig. 2. Bright field image under two beam condition with $\mathrm{g} = 002$ (sample V10). Nonuniform distribution of coherent precipitates with butterfly diffraction contrast can be observed.

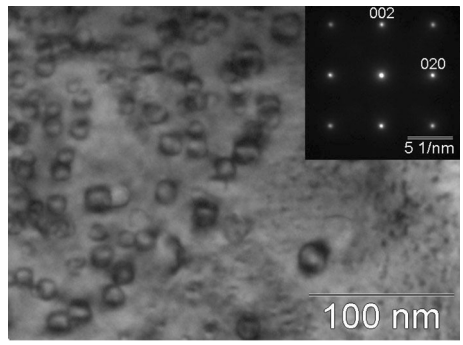

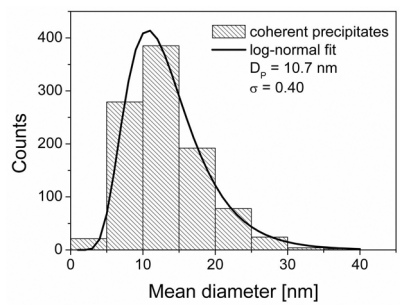

Fig. 3. Coherent precipitates in sample V10. (Top) Ring-shape coherent precipitates under bright field imaging from [100] zone axis (inset). (Bottom) Coherent precipitates size histogram and its log-normal fitting.

reported in these rapidly cooled alloys. Typical butterfly diffraction contrast due to lattice mismatch with the matrix indicates a fine dispersion of coherent precipitates. In the case of Fig. 2, taken under two beam condition, the width of the strain contrast around the coherent precipitates is broad. To measure the size of these precipitates, bright field zone axis imaging (BFZA) was used. Fig. 3(a) shows small coherent precipitates recognized by their ring-shape strain contrast [9] when studied under BFZA condition. Fig. 3(b) presents the precipitate size histogram and the corresponding log-normal distribution fitting, from which the mean precipitate diameter $D_P = 10.7$ nm and the distribution width $\sigma = 0.4$ were obtained.

Larger, round precipitates of about 40 nm were observed in the coherent precipitate free zone. They were identified as CoO particles by extra reflections in the electron diffraction patterns

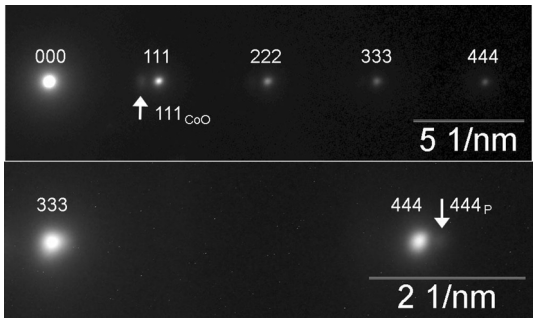

Fig. 4. SAED pattern of a 111 systematic row in sample V10. (Top) Low exposure image showing the 111 CoO extra reflection. (Bottom) Large exposure image of the faint reflections in a) showing the 444_P reflection, corresponding to the coherent precipitates.

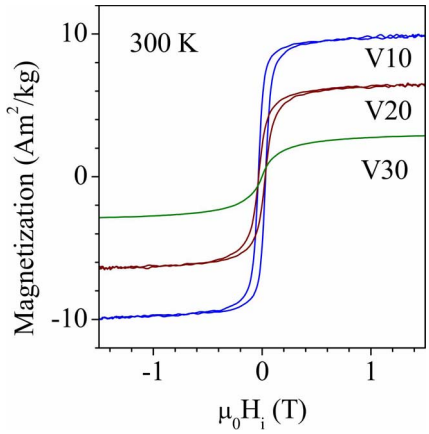

Fig. 5. Room temperature hysteresis loops of the alloy quenched at different rates. Sample V30 is superparamagnetic while the magnetic polarization of samples V20 and V10 have two contributions: a superparamagnetic and a ferromagnetic one.

[Fig. 4(a)], dark field contrast and EDS. To search for additional reflections corresponding to the coherent precipitates, higher order reflections were excited, as for example $\mathrm{g} = 444$ in Fig. 4(a). A large exposure image of reflection 333 and 444 reveals an additional spot corresponding to the coherent precipitates [Fig. 4(b)] which is in agreement with XRD data. EDS analysis on the coherent precipitates reveals an enhanced Co peak.

The room temperature magnetic hysteresis loops shown in Fig. 5 were fitted by the addition of a superparamagnetic M_{SPM} and a ferromagnetic M_{FM} contribution as [7]

$$M_{\mathrm{FM}} = \frac{2M_{\mathrm{SF}}}{\pi}\left[\arctan\left(\frac{H_i}{H_{\mathrm{iC}}}\right)\tan\frac{\pi M_R}{M_{\mathrm{sf}}}\right] \quad (1)$$

$$M_{\mathrm{SPM}} = M_{\mathrm{SP}}\left[\coth\left(\frac{\mu_P H_i}{k_B T}\right) - \frac{k_B T}{\mu_P H_i}\right] \quad (2)$$

where M_{SF} and M_{SP} are the ferromagnetic and superparamagnetic saturation magnetizations, respectively, $\mu_0 H_{iC}$ the internal coercive field, M_R the remanent magnetization, and μ_P the magnetic moment of the superparamagnetic units. Sample V30 is superparamagnetic but samples V20 and V10 are better described by considering both contributions. Assuming that the paramagnetic units are Co clusters, the mean particle size $d_{\mathrm{Loop}}(= (\mu_P/(\mu_0 M_S(\mathrm{Co}))^{1/3})$ is estimated (see Table II). The antiferromagnetic CoO phase is expected to influence weakly the overall magnetization values.

The low field magnetization versus temperature behavior and the blocking temperature distribution in the samples were investigated by measuring magnetization versus temperature curves (see Fig. 6) following the ZFC-FC protocol, under a constant field of 10 mT. The curve for sample V10 is consistent with a wide distribution of blocking temperatures, with a certain fraction of ferromagnetic particles, while V20 and V30 exhibit the maximum in the ZFC curve at low temperature—15 K (V20) and 14 K (V30)—indicating a superparamagnetic contribution. The resulting blocking temperature distributions are shown in Fig. 7. These distributions were fitted by log-normal functions [10]; the mean particle size estimated from the distributions d_1 and d_2 (considering the precipitates as pure Co) are listed in Table II. It is worth noting that the precipitate sizes obtained from the analysis of the hysteresis loop are somewhat larger

TABLE II
PRECIPITATE MEAN SIZE ESTIMATED USING DIFFERENT ROUTES

Sample	D_P [nm]	D_{CoO} [nm]	d_{Loop} [nm]	d_1 [nm]	d_2 [nm]
V10	10.7(4)	40	4.5(5)	1.8	3.9
V20	-	-	6.5(5)	1.6	2.7
V30	-	-	2.3(5)	0.6	1.6

Precipitate size estimated assuming properties corresponding to pure Co. Included in this table are: the small coherent Co rich D_P and large CoO D_{CoO} precipitate sizes obtained with TEM; the mean size of precipitates contributing to the superparamagnetic component of the hysteresis loop d_{Loop} and the precipitate size d_1 and d_2 estimated from Fig. 7.

TABLE III
HYSTERESIS LOOP PARAMETERS

Sample	J_{SF} [T]	$\mu_0 H_{iC}$ [T]	J_R [T]	$S = J_R/J_{SF}$	J_{SP} [T]
V10	0.1015	0.0413	0.0547	0.54	0.0303
V20	0.0722	0.0332	0.0227	0.31	0.0191
V30	-	-	-	-	0.0239

than those calculated from the M versus T curves. This may be due to the fact that only particles which are superparamagnetic at room temperature are considered in the first one while in the other case the complete distribution of blocking temperatures is swept.

Concerning the hysteresis behavior, many precipitates P are large enough to be blocked even at room temperature (the critical superparamagnetic size is about 6 nm at 300 K) so the large Co-rich particles are likely to be responsible for the ferromagnetic contribution to the hysteresis loop; however, the measured room temperature coercivity of about 30–50 mT is well below the values predicted (about 0.3 T [11]) for an ensemble of non-interacting single domain particles changing the magnetic polarization by a mechanism of coherent spin rotation inside the precipitates.

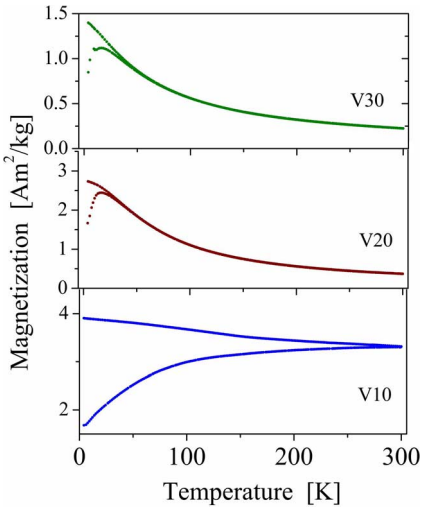

Fig. 6. Low field (10 mT) magnetic polarization as a function of temperature in the ZFC and FC conditions.

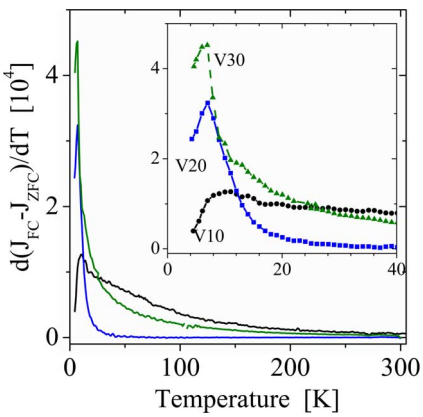

Fig. 7. Blocking temperature distributions calculated from data in Fig. 6.

IV. Conclusion

$Cu_{90}Co_{10}$ alloys have been produced with the technique of twin roller melt spinning, applying a contact force between the two rolling wheels of 24 N. Samples quenched at high rates (V30) are superparamagnetic showing no evidence of interactions in the J versus H curves at room temperature. As the quenching rate decreases, two precipitate families are observed by TEM: small coherent Cu(Co) precipitates forming colonies and larger CoO ones (∼40 nm), found in the coherent precipitate free zones between these colonies. The hysteresis loops of samples quenched at lower rates (V20 and V10) are consistent with two contributions, with a soft ferromagnetic component in addition to the superparamagnetic one. Relatively small coercivity values, of about 30–50 mT, are measured at room temperature in the as-cast state, which cannot be addressed by a coherent spin rotation mechanism inside the Co-rich precipitates.

Acknowledgment

This work was supported in part by CONICET and SECyT-UNC. The authors would like to express their gratitude to Dr. A. J. Tolley for his valuable help and fruitful discussion.

References

[1] A. E. Berkowitz, J. R. Mitchell, M. J. Carey, A. P. Young, S. Zhang, F. E. Spada, F. T. Parker, A. Hutten, and G. Thomas, "Giant magnetoresistance in heterogeneous Cu-Co alloys," *Phys. Rev. Lett.*, vol. 68, p. 3745, 1992.

[2] J. Wecker, R. von Helmott, L. Schultz, and K. Samwer, "Giant magnetoresistance in melt spun Cu-Co alloyss," *Appl. Phys. Lett.*, vol. 62, no. 16, p. 19985, 1993.

[3] R. Busch, F. Gartner, C. Borchers, P. Haasen, and R. Bormann, "Microstructure development during rapid solidification of highly supersaturated Cu-Co alloys," *Acta Mater.*, vol. 43, p. 3467, 1995.

[4] P. Panissod, M. Malinowska, E. Jedryka, M. Wojcik, S. Nadolski, M. Knobel, and J. E. Schmidt, "Inhomogeneous structure and magnetic properties of granular $Co_{10}Cu_{90}$ alloys," *Phys. Rev. B*, vol. 63, p. 014408, 2000.

[5] M. G. M. Miranda, E. Estévez-Rams, G. Martínez, and M. N. Baibich, "Phase separation in $Cu_{90}Co_{10}$ high-magnetoresistance materials," *Phys. Rev. B*, vol. 68, p. 014434, 2003.

[6] E. F. Ferrari, F. C. S. da Silva, and M. Knobel, "Theory of giant magnetoresistance in granular alloys," *Phys. Rev. B*, vol. 59, no. 13, p. 8412, 1999.

[7] L. M. Fabietti and S. E. Urreta, "Structure and magnetic properties of Cu-10 wt% Co alloys processed by twin roller melt spinning," *Physica B*, vol. 398, pp. 348–351, 2007.

[8] L. M. Fabietti, J. Ferreyra, M. Villafuerte, S. E. Urreta, and S. P. Heluani, "Kondo-like effect in magnetoresistive CuCo alloys," *Phys. Rev. B*, vol. 82, p. 172410, 2010.

[9] R. Hattenhauer and F. Haider, "Improved imaging of small coherent precipitates by bright field/zone axis incidence TEM," *Scr. Metall. Mater.*, vol. 25, p. 1173, 1991.

[10] M. Knobel, L. M. Socolovsky, and J. M. Vargas, "Propiedades magnéticas y de transporte de sistemas nanocristalinos: Conceptos básicos y aplicaciones a sistemas reales," *Revista Mexicana de Física E*, vol. 50, no. 1, pp. 8–28, 2004.

[11] R. C. O'Handley, *Modern Magnetic Materials. Principles and Applications*, 1st ed. New York, NY, USA: Wiley, 2000, p. 323.